Mn K-Edge XANES and Kβ XES Studies of Two Mn−Oxo Binuclear Complexes: Investigation of Three Different Oxidation States Relevant to the Oxygen-Evolving Complex of Photosystem II

Hendrik Visser,[†,‡] Elodie Anxolabéhère-Mallart,[*,†,||] Uwe Bergmann,[†,§] Pieter Glatzel,[†,§] John H. Robblee,[†,‡] Stephen P. Cramer,[*,†,§] Jean-Jacques Girerd,[||] Kenneth Sauer,[*,†,‡] Melvin P. Klein,[†] and Vittal K. Yachandra[*,†]

Contribution from the Melvin Calvin Laboratory, Physical Biosciences Division, Lawrence Berkeley National Laboratory, Berkeley, California 94720, Department of Chemistry, University of California, Berkeley, California 94720-5230, Department of Applied Science, University of California, Davis, California 95616, and Laboratoire de Chimie Inorganique, UMR CNRS 8613, Université de Paris-Sud, 91405 Orsay, France

Received December 20, 2000. Revised Manuscript Received April 12, 2001

Abstract: Two structurally homologous Mn compounds in different oxidation states were studied to investigate the relative influence of oxidation state and ligand environment on Mn K-edge X-ray absorption near-edge structure (XANES) and Mn Kβ X-ray emission spectroscopy (Kβ XES). The two manganese compounds are the di-μ-oxo compound $[L'_2Mn^{III}O_2Mn^{IV}L'_2](ClO_4)_3$, where L′ is 1,10-phenanthroline (Cooper, S. R.; Calvin, M. *J. Am. Chem. Soc.* **1977**, *99*, 6623−6630) and the linear mono-μ-oxo compound $[LMn^{III}OMn^{III}L](ClO_4)_2$, where L^- is the monoanionic *N*,*N*-bis(2-pyridylmethyl)-*N*′-salicylidene-1,2-diaminoethane ligand (Horner, O.; Anxolabéhère-Mallart, E.; Charlot, M. F.; Tchertanov, L.; Guilhem, J.; Mattioli, T. A.; Boussac, A.; Girerd, J.-J. *Inorg. Chem.* **1999**, *38*, 1222−1232). Preparative bulk electrolysis in acetonitrile was used to obtain higher oxidation states of the compounds: the $Mn^{IV}Mn^{IV}$ species for the di-μ-oxo compound and the $Mn^{III}Mn^{IV}$ and $Mn^{IV}Mn^{IV}$ species for the mono-μ-oxo compound. IR, UV/vis, EPR, and EXAFS spectra were used to determine the purity and integrity of the various sample solutions. The Mn K-edge XANES spectra shift to higher energy upon oxidation when the ligand environment remains similar. However, shifts in energy are also observed when only the ligand environment is altered. This is achieved by comparing the di-μ-oxo and linear mono-μ-oxo Mn−Mn moieties in equivalent oxidation states, which represent major structural changes. The magnitude of an energy shift due to major changes in ligand environment can be as large as that of an oxidation-state change. Therefore, care must be exercised when correlating the Mn K-edge energies to manganese oxidation states without taking into account the nature of the ligand environment and the overall structure of the compound. In contrast to Mn K-edge XANES, Kβ XES spectra show less dependence on ligand environment. The K$\beta_{1,3}$ peak energies are comparable for the di-μ-oxo and mono-μ-oxo compounds in equivalent oxidation states. The energy shifts observed due to oxidation are also similar for the two different compounds. The study of the different behavior of the XANES pre-edge and main-edge features in conjunction with Kβ XES provides significant information about the oxidation state and character of the ligand environment of manganese atoms.

Introduction

In green plants and cyanobacteria, light-induced water oxidation is performed by a membrane-bound protein cluster, photosystem II (PS II). This protein cluster contains an active site, the oxygen-evolving complex (OEC), where water binds and is oxidized during four consecutive photon-induced electron extractions. In the absence of high-resolution crystallographic information, most of the structural information about the OEC comes from X-ray absorption spectroscopy (XAS) and EPR studies on PS II[3−11] and on model complexes.[1,12−16] These techniques have been used to investigate both the structure of the OEC and the mechanism of water oxidation.[17−22] The

* To whom correspondence should be addressed. E-mail: SPCramer@lbl.gov, KHSauer@lbl.gov, VKYachandra@lbl.gov, or Eanxolab@icmo.u-psud.fr.

† Lawrence Berkeley National Laboratory.

‡ University of California, Berkeley.

§ University of California, Davis.

|| Université de Paris-Sud.

(1) Cooper, S. R.; Calvin, M. *J. Am. Chem. Soc.* **1977**, *99*, 6623−6630.

(2) Horner, O.; Anxolabéhère-Mallart, E.; Charlot, M. F.; Tchertanov, L.; Guilhem, J.; Mattioli, T. A.; Boussac, A.; Girerd, J.-J. *Inorg. Chem.* **1999**, *38*, 1222−1232.

(3) Kirby, J. A.; Goodin, D. B.; Wydrzynski, T.; Robertson, A. S.; Klein, M. P. *J. Am. Chem. Soc.* **1981**, *103*, 5537−5542.

(4) Yachandra, V. K.; Sauer, K.; Klein, M. P. *Chem. Rev.* **1996**, *96*, 2927−2950.

(5) Liang, W.; Roelofs, T. A.; Cinco, R. M.; Rompel, A.; Latimer, M. J.; Yu, W. O.; Sauer, K.; Klein, M. P.; Yachandra, V. K. *J. Am. Chem. Soc.* **2000**, *122*, 3399−3412.

(6) Penner-Hahn, J. E. *Struct. Bonding (Berlin)* **1998**, *90*, 1−36.

(7) Liang, W.; Latimer, M. J.; Dau, H.; Roelofs, T. A.; Yachandra, V. K.; Sauer, K.; Klein, M. P. *Biochemistry* **1994**, *33*, 4923−4932.

(8) Miller, A. F.; Brudvig, G. W. *Biochim. Biophys. Acta* **1991**, *1056*, 1−18.

(9) Messinger, J.; Robblee, J. H.; Yu, W. O.; Sauer, K.; Yachandra, V. K.; Klein, M. P. *J. Am. Chem. Soc.* **1997**, *119*, 11349−11350.

(10) Peloquin, J. M.; Britt, R. D. *Biochim. Biophys. Acta* **2001**, *1503*, 96−111.

(11) Robblee, J. H.; Cinco, R. M.; Yachandra, V. K. *Biochim. Biophys. Acta* **2001**, *1503*, 7−23.

(12) Kirby, J. A.; Robertson, A. S.; Smith, J. P.; Thompson, A. C.; Cooper, S. R.; Klein, M. P. *J. Am. Chem. Soc.* **1981**, *103*, 5529−5537.

(13) Wieghardt, K. *Angew. Chem., Int. Ed. Engl.* **1989**, *28*, 1153−1172.

10.1021/ja004306h CCC: $20.00
Published on Web 06/29/2001

consensus is that the OEC contains four manganese atoms, consisting of two to three di-μ-oxo Mn−Mn moieties and one mono-μ-oxo Mn−Mn moiety. Kok et al.[23] proposed that water is oxidized in five stages, called S-states (S_0-S_4), with the index indicating the number of stored oxidizing equivalents. An electron is extracted during each of the first four light-induced transitions, $S_0\rightarrow S_1$, $S_1\rightarrow S_2$, $S_2\rightarrow S_3$, and $S_3\rightarrow[S_4]\rightarrow S_0$. Dioxygen is released during the last transition, when the S_3 state returns to the S_0 state via the hypothesized S_4 state.

To understand the mechanism of water oxidation in more detail, it is important to know at each stage whether the extracted electrons are coming directly from bound water, from the Mn atoms, or from any other parts of the OEC. Both EPR and Mn K-edge X-ray absorption near-edge structure (XANES) have been used extensively to investigate the involvement of the Mn atoms in water oxidation. On the basis of the results of these techniques, there is consensus that Mn is oxidized during the $S_0\rightarrow S_1$ and $S_1\rightarrow S_2$ transitions. However, there is still controversy concerning the involvement of Mn oxidation in the $S_2\rightarrow S_3$ transition. Roelofs et al.[24] concluded that there is no Mn oxidation in the $S_2\rightarrow S_3$ transition, on the basis of the absence of a significant shift in the XANES spectra between S_2 and S_3, and proposed that a ligand is oxidized. However, Ono et al.[25] and Iuzzolino et al.[26] concluded, on the basis of observed shifts in their XANES data, that Mn oxidation is involved in this transition.

Recently, Messinger et al.[22] performed a modified version of the experiment done by Roelofs et al.,[24] using XANES and an additional technique, Kβ X-ray emission spectroscopy (Kβ XES).[27,28] Like XANES, Kβ XES is element-specific, but in comparison to XANES it has the advantage that it is more sensitive to the oxidation state and less sensitive to the ligand environment of the manganese atoms.

XANES results from the excitation of a 1s electron (K-shell) to a higher, bound orbital (Figure 1). The higher the oxidation state of the metal, the more positive the overall charge of the atom, and more energy is required to excite an electron out of an orbital.[29] The first formally allowed electric dipole transition is the 1s→4p transition. Due to the size of the 4p orbital, it overlaps with p orbitals of the ligands, either through σ- or π-bonding. Consequently, this transition is sensitive to the oxidation state and the ligand environment of the metal. For certain symmetries around the metal, the formally electric-dipole forbidden 1s→3d transition can be observed, occurring at a lower energy than the main edge transitions.[30] This transition gains intensity due to mixing of metal 3d and 4p orbitals, and gives information about the ligand as well as about the oxidation state and symmetry of the metal complex.[31,32] To increase the sensitivity of XANES, absorption is detected as an excitation spectrum by measuring the Kα fluorescence of the Mn atoms.[33]

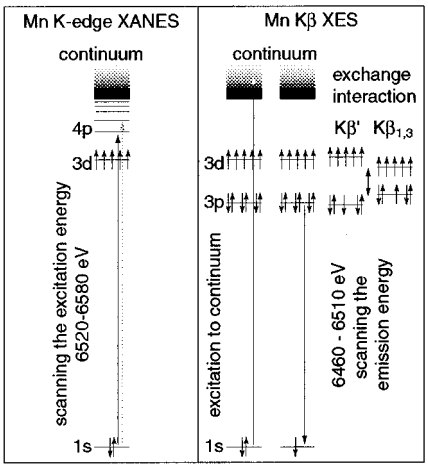

Figure 1. A schematic for the excitation and emission processes involved in XANES and Kβ XES spectroscopy. XANES spectra reflect the transition energy of 1s electrons excited to higher bound states, which depends on the overall charge and ligand environment of the metal.[29] To enhance sensitivity, the absorption spectra are collected as excitation spectra using Mn Kα fluorescence detection. Kβ XES arise from the emission of a 3p electron to 1s hole, which is formed following X-ray absorption. In a simplified model, two final spin states exist with either a constructive (K$\beta_{1,3}$) or destructive (Kβ') spin exchange interaction between the unpaired 3p and 3d electrons. The magnitude of the interaction depends on the number of unpaired 3d electrons, which is related to the oxidation state of high-spin Mn. For a more accurate model, the ligand-field multiplet formalism needs to be applied, taking into account spin−spin and spin−orbit interactions, ligand-field splitting, and Jahn−Teller distortions.[28]

In contrast to XANES, Kβ XES detects the X-ray emission from the relaxation of a 3p electron to a 1s hole, which is created by excitation of a 1s electron into the continuum (Figure 1). In a simplified model, two final states exist due to a constructive (K$\beta_{1,3}$) or destructive (Kβ') spin-exchange interaction between the unpaired electrons in the 3p and 3d orbitals.[34,35] The magnitude of the exchange interaction depends on the number of unpaired electrons in the 3d orbital. Increasing the oxidation state of high-spin Mn decreases the number of unpaired 3d

(14) Pecoraro, V. L.; Baldwin, M. J.; Gelasco, A. *Chem. Rev.* **1994**, *94*, 807−826.
(15) Cinco, R. M.; Rompel, A.; Visser, H.; Aromí, G.; Christou, G.; Sauer, K.; Klein, M. P.; Yachandra, V. K. *Inorg. Chem.* **1999**, *38*, 5988−5998.
(16) Pecoraro, V. L.; Hsieh, W.-Y. In *Manganese and Its Role in Biological Processes*; Sigel, A., Sigel, H., Eds.; Marcel Dekker Inc.: New York, 2000; Vol. 37, pp 429−504.
(17) Christou, G.; Vincent, J. B. *Biochim. Biophys. Acta* **1987**, *895*, 259−274.
(18) Renger, G. *Physiol. Plant.* **1997**, *100*, 828−841.
(19) Hoganson, C. W.; Babcock, G. T. *Science* **1997**, *277*, 1953−1956.
(20) Haumann, M.; Junge, W. *Biochim. Biophys. Acta* **1999**, *1411*, 86−91.
(21) Siegbahn, P. E. M.; Crabtree, R. H. *J. Am. Chem. Soc.* **1999**, *121*, 117−127.
(22) Messinger, J.; Robblee, J. H.; Bergmann, U.; Fernandez, C.; Glatzel, P.; Visser, H.; Cinco, R. M.; McFarlane, K. L.; Bellacchio, E.; Pizarro, S. A.; Cramer, S. P.; Sauer, K.; Klein, M. P.; Yachandra, V. K. *J. Am. Chem. Soc.* **2001**, in press.
(23) Kok, B.; Forbush, B.; McGloin, M. *Photochem. Photobiol.* **1970**, *11*, 457−475.
(24) Roelofs, T. A.; Liang, M. C.; Latimer, M. J.; Cinco, R. M.; Rompel, A.; Andrews, J. C.; Sauer, K.; Yachandra, V. K.; Klein, M. P. *Proc. Natl. Acad. Sci. U.S.A.* **1996**, *93*, 3335−3340.
(25) Ono, T.; Noguchi, T.; Inoue, Y.; Kusunoki, M.; Matsushita, T.; Oyanagi, H. *Science* **1992**, *258*, 1335−1337.
(26) Iuzzolino, L.; Dittmer, J.; Dörner, W.; Meyer-Klaucke, W.; Dau, H. *Biochemistry* **1998**, *37*, 17112−17119.
(27) Stojanoff, V.; Hämäläinen, K.; Siddons, D. P.; Hastings, J. B.; Berman, L. E.; Cramer, S.; Smith, G. *Rev. Sci. Instrum.* **1992**, *63*, 1125−1127.
(28) Peng, G.; DeGroot, F. M. F.; Hämäläinen, K.; Moore, J. A.; Wang, X.; Grush, M. M.; Hastings, J. B.; Siddons, D. P.; Armstrong, W. H.; Mullins, O. C.; Cramer, S. P. *J. Am. Chem. Soc.* **1994**, *116*, 2914−2920.
(29) Shulman, R. G.; Yafet, Y.; Eisenberger, P.; Blumberg, W. E. *Proc. Natl. Acad. Sci. U.S.A.* **1976**, *73*, 1384−1388.
(30) Roe, A. L.; Schneider, D. J.; Mayer, R. J.; Pyrz, J. W.; Widom, J.; Que, L., Jr. *J. Am. Chem. Soc.* **1984**, *106*, 1676−1681.
(31) DuBois, J. L.; Mukherjee, P.; Stack, T. D. P.; Hedman, B.; Solomon, E. I.; Hodgson, K. O. *J. Am. Chem. Soc.* **2000**, *122*, 5775−5787.
(32) Westre, T. E.; Kennepohl, P.; DeWitt, J. G.; Hedman, B.; Hodgson, K. O.; Solomon, E. I. *J. Am. Chem. Soc.* **1997**, *119*, 6297−6314.
(33) Jaklevic, J.; Kirby, J. A.; Klein, M. P.; Robertson, A. S.; Brown, G. S.; Eisenberger, P. *Solid State Commun.* **1977**, *23*, 679−682.
(34) Tsutsumi, K.; Nakamori, H. *J. Phys. Soc. Jpn.* **1968**, *25*, 1419−1424.
(35) Tsutsumi, K.; Nakamori, H.; Ichikawa, K. *Phys. Rev. B: Condens. Matter* **1976**, *13*, 929−933.

electrons, in the high spin case; concomitantly, the spin-exchange interaction decreases. Accordingly, the K$\beta_{1,3}$ transition shifts to a higher, and the Kβ' transition shifts to a lower, energy.[28,36−38] Compared to the 4p orbitals, the 3p orbitals have less overlap with the ligand orbitals, because they are smaller and more buried within the electronic shells. Therefore, Kβ XES is less sensitive to the ligand environment compared to XANES. The K$\beta_{1,3}$ transition is better resolved than the Kβ' transition due to a difference in relaxation processes.[39] Hence, the K$\beta_{1,3}$ transition is used here as a indicator of the oxidation state of the metal.

A more accurate view on Kβ XES requires the ligand-field multiplet formalism. For example, in the atomic picture, a Mn^{II} atom has five 3d electrons (^{6}S term state) and one unpaired 3p electron (^{2}S) after Kβ emission. A variety of spin multiplet states exists when the spin−spin exchange interaction is included; two of the main states are the ^{7}P (part of K$\beta_{1,3}$) and the ^{5}P (part of Kβ') symmetry. Using this formalism enables inclusion of other symmetry-dependent perturbations such as spin−orbit coupling, ligand-field splitting, Jahn−Teller distortion, and in case of multinuclear compounds, spin−spin interaction between different metal atoms. Each of these perturbations will split the spin states into a multiplet of states, causing an asymmetric broadening of the observed emission peaks. This indicates that there is some dependence of the ligand environment on Kβ XES spectra.

On the basis of the results from both of these techniques, it was concluded that no manganese oxidation accompanies the $S_2 \rightarrow S_3$ transition.[22] Nevertheless, some supporters of manganese oxidation in the $S_2 \rightarrow S_3$ transition argue that two opposing effects cause the lack of a shift in XANES and Kβ XES data. A structural change occurs in the OEC during the $S_2 \rightarrow S_3$ transition,[5] which could offset the effects due to manganese oxidation. To resolve this issue, the influence of oxidation state and structural changes on XANES and Kβ XES spectra needs to be established. To address this question, two manganese compounds in solution are studied here to investigate the influence of oxidation state versus ligand environment on XANES and Kβ XES data. The structural differences between the two chosen compounds are much greater than that observed between the S_2 and S_3 states as detected by EXAFS.[5]

The two compounds studied are the di-μ-oxo-bridged compound $[L'_2Mn^{III}O_2Mn^{IV}L'_2](ClO_4)_3$, where L′ is 1,10-phenanthroline[1] (Figure 2A) and the mono-μ-oxo bridged compound $[LMn^{III}OMn^{III}L](ClO_4)_2$, where L^- is the monoanionic *N*,*N*-bis(2-pyridylmethyl)-*N*′-salicylidene-1,2-diaminoethane ligand[2] (Figure 2B). The di-μ-oxo compound has a diamond-core $Mn^{III}-O_2-Mn^{IV}$ unit with a Mn−Mn distance of 2.75 Å. One reversible wave is observed in the cyclic voltammetry at $E^{1/2} = +1.26$ V vs SCE of a $[(L')_2Mn^{III}O_2Mn^{IV}(L')_2]^{3+}$ acetonitrile solution for the ($Mn^{III}Mn^{IV} \leftrightarrows Mn^{IV}Mn^{IV} + e^-$) couple.[1,40,41] The mono-μ-oxo compound contains a linear $Mn^{III}-O-Mn^{III}$ unit with a Mn−Mn distance of 3.52 Å. Cyclic voltammetry of a solution of $[LMn^{III}OMn^{III}L]^{2+}$ in acetonitrile shows two reversible waves at $E_1^{1/2} = +0.54$ V vs SCE and at $E_2^{1/2} = +0.99$ V vs SCE for the ($Mn^{III}Mn^{III} \rightleftarrows Mn^{III}Mn^{IV} + e^-$) and ($Mn^{III}Mn^{IV} \rightleftarrows Mn^{IV}Mn^{IV} + e^-$) couples, respectively.[42−45]

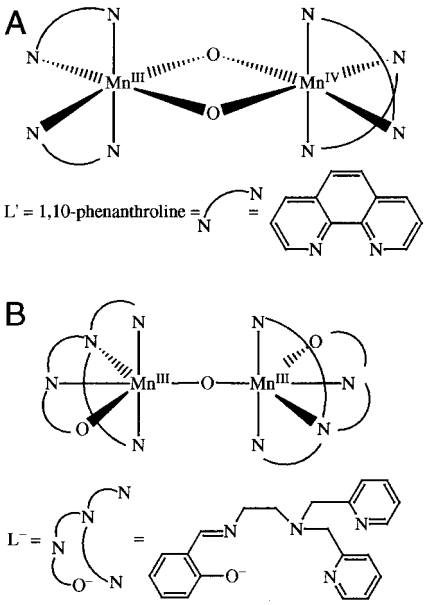

Figure 2. (A) The di-μ-oxo manganese compound $[L'_2\ Mn^{III}O_2Mn^{IV}L'_2]^{3+}$, with L′ as 1,10-phenanthroline.[1,40,41] (B) The linear mono-μ-oxo compound, $[LMn^{III}OMn^{III}L]^{2+}$, with L^- as the monoanionic *N*,*N*-bis(2-pyridylmethyl)-*N*′-salicylidene-1,2-diaminoethane ligand.[2,42]

Samples of the different oxidation states of both compounds are made by preparative bulk electrolysis. To determine the extent of the influence of oxidation state and ligand environment on the Mn K-edge XANES and Kβ XES spectra, pure oxidation-state compound spectra are required. However, the electrochemical preparation of the different oxidation states for each compound is not 100% complete. Therefore, UV/vis and EPR spectroscopies are used to determine the manganese species present in the electrochemical solutions. This information is used to deconvolute the measured spectra into pure oxidation-state compound spectra. EXAFS spectroscopy is used as an additional tool to verify the integrity of the electrochemically prepared compounds. By comparing the different oxidation states for each compound, the effect of manganese oxidation on XANES and Kβ XES data is studied. The influence of ligands is investigated by comparing the spectra of the two compounds in equivalent manganese oxidation states. This is the first such study of structurally homologous oxo-bridged Mn compounds in different oxidation states to be studied by XAS and Kβ XES methodology.

Experimental Section

Preparation of Di-μ-oxo Compound Samples. Synthesis of the di-μ-oxo compound, $[L'_2Mn^{III}O_2Mn^{IV}L'_2](ClO_4)_3$ with L′ as 1,10-phenanthroline, is adapted from the published procedure by Cooper et al.[1] The IR spectrum of the recrystallized solid compound was recorded to determine the purity, and it matches the published data.[1] Electrochemistry of $[L'_2Mn^{III}O_2Mn^{IV}L'_2]^{3+}$ in acetonitrile shows one anodic wave at +1.26 V vs SCE, corresponding to the ($Mn^{III}Mn^{IV} \leftrightarrows$

(36) Sanner, V. H. Ph.D. thesis, Uppsala University, 1941.
(37) Tsutsumi, K. *J. Phys. Soc. Jpn.* **1959**, *14*, 1696−1706.
(38) Urch, D. S.; Wood, P. R. *X-ray Spectrom.* **1978**, *7*, 9−11.
(39) Taguchi, M.; Uozumi, T.; Kotani, A. *J. Phys. Soc. Jpn.* **1997**, *66*, 247−256.
(40) Stebler, M.; Ludi, A.; Bürgi, H.-B. *Inorg. Chem.* **1986**, *25*, 4743−4750.
(41) Manchanda, R.; Brudvig, G. W.; Degala, S.; Crabtree, R. H. *Inorg. Chem.* **1994**, *33*, 5157−5160.
(42) Anxolabéhère-Mallart, E.; Visser, H.; Bergman, U.; Cramer, S. P.; Girerd, J.-J.; Sauer, K.; Yachandra, V. K.; Klein, M. P. *J. Inorg. Biochem.* **1999**, *74*, 66.
(43) Poussereau, S. Ph.D. Thesis, Université de Paris-Sud, 1999.
(44) Albela, B.; Chottard, G.; Girerd, J.-J. *J. Biol. Inorg. Chem.* **2001**, *6*, 430−434.
(45) Although the cation resulting from the second oxidation process has been shown to possess some phenoxyl radical character,[2,44,46] further experiments showed that this radical is not stable and that it evolves rapidly into the $[Mn^{IV}Mn^{IV}]^{4+}$ cation.[43,44]

$Mn^{IV}Mn^{IV} + e^-$) couple. The $[L'_2Mn^{IV}O_2Mn^{IV}L'_2]^{4+}$ cation is prepared from a 1.7×10^{-4} M $Mn^{III}Mn^{IV}$ di-μ-oxo compound solution at +1.4 V vs SCE under an argon atmosphere at room temperature. Figure 3 shows a scheme of the two compound fractions as a function of time during electrolysis. Samples are extracted at different times for XAS, Kβ XES, UV/vis, and quantitative EPR. In the nomenclature of the electrochemical samples, "**di**" refers to the di-μ-oxo compound, and "**mono**" refers to the mono-μ-oxo compound. The Roman numerals between brackets indicate the desired oxidation state of the compound. Different extraction time-points are indicated by subscripts. The samples from the di-μ-oxo compound,$[L'_2Mn^{III}O_2Mn^{IV}L'_2]$ $(ClO_4)_3$, are designated **di(III,IV)**, **di(IV,IV)$_A$**, and **di(IV,IV)$_B$**.

The starting $Mn^{III}Mn^{IV}$ di-μ-oxo compound is EPR-active ($S = {}^1/_2$, with a distinctive 16-line spectrum), and the $Mn^{IV}Mn^{IV}$ species is EPR-silent ($S = 0$).[47] Therefore, the EPR spectra of the **di(IV,IV)** samples are used to determine the degree of completion of the oxidation step by measuring the decline in the $Mn^{III}Mn^{IV}$ species. The EPR data are included in the Supporting Information.

Preparation of Mono-μ-oxo Compound Samples. Synthesis of the mono-μ-oxo compound, $[LMn^{III}OMn^{III}L](ClO_4)_2$ with L^- as the monoanionic *N*,*N*-bis(2-pyridylmethyl)-*N*′-salicylidene-1,2-diaminoethane ligand is according to the procedure by Horner et al.[2] The mono-μ-oxo compound is recrystallized, and it was determined that the IR spectrum agrees with the published data.[2] Cyclic voltammetry of $[LMn^{III}OMn^{III}L]^{2+}$ in acetonitrile shows two reversible anodic waves at: +0.54 V vs SCE for the ($Mn^{III}Mn^{III} \leftrightharpoons Mn^{III}Mn^{IV} + e^-$) couple and at +0.99 V vs SCE for the ($Mn^{III}Mn^{IV} \leftrightharpoons Mn^{IV}Mn^{IV} + e^-$) couple.[2,42] The cation $[LMn^{III}OMn^{IV}L]^{3+}$ is prepared from a 5.0×10^{-4} M $Mn^{III}Mn^{III}$ mono-μ-oxo compound solution by bulk electrolysis at $E = +0.85$ V vs SCE under argon atmosphere at −35 °C. To prepare the $[LMn^{IV}OMn^{IV}L]^{4+}$ cation, the potential is raised to +1.3 V vs SCE. Figure 4 shows a scheme of the different mono-μ-oxo compound fractions during the two electrochemical steps, and the sample extraction time points. The samples from the mono-μ-oxo compound, $[LMn^{III}OMn^{III}L](ClO_4)_2$, are designated by **mono(III,III)**, **mono(III,IV)**, and **mono(IV,IV)$_A$** through **mono(IV,IV)$_F$**.

UV/vis absorption spectroscopy is used to determine the extent of the first oxidation step (sample **mono(III,IV)**), that is, the ratio between the $Mn^{III}Mn^{III}$ and $Mn^{III}Mn^{IV}$ species. To monitor the progress of the second oxidation step, EPR spectroscopy is used, because the $Mn^{III}Mn^{IV}$ species has a distinctive 16-line spectrum ($S = {}^1/_2$) and the $Mn^{III}Mn^{III}$ and $Mn^{IV}Mn^{IV}$ species are both EPR-silent ($S = 0$). Using this signal, the EPR spectra of the **mono(IV,IV)** samples are analyzed to determine the decline in the $Mn^{III}Mn^{IV}$ fraction. When water is present in the electrolyte, the $Mn^{IV}Mn^{IV}$ species is unstable[2] and decomposes into Mn^{II}, which has a distinctive six-line EPR signal ($S = {}^5/_2$). Therefore, EPR is also used to correct the $Mn^{IV}Mn^{IV}$ fraction for this small amount of decomposition (3%) of the **mono(IV,IV)** samples. The details of the quantitation procedures using UV/vis and EPR spectroscopy are presented in the Supporting Information.

Cyclic Voltammetry and Bulk Electrolysis. For electrochemical experiments an electrolyte solution of 0.2 M tetrabutylammonium perchlorate (Puriss Fluka) in high-quality acetonitrile (Burdick & Jackson) is used. For each complex, cyclic voltammetry is run before electrolysis. A platinum disk of 1.5 mm diameter is used as a working electrode for cyclic voltammetry. For bulk electrolysis in a double-jacketed cylindrical cell, a cylindrical Pt grid of about 20 mm diameter is used as a working electrode. The auxiliary electrode is made of a Pt grid in a glass tube with a fritted glass disk at the end to separate the electrode from the sample solution. The reference electrode is Ag/$AgClO_4$ in 0.1 M TBA(ClO_4) acetonitrile (270 mV more positive than SCE). Cyclic voltammetry and bulk electrolysis are conducted using a BAS CV-27 voltammetry controller. Bulk electrolysis is performed at room temperature for the di-μ-oxo compound and at −35 °C for the mono-μ-oxo compound.

To minimize degradation during electrochemistry, the electrolyte solution is dried by running it through an Al_2O_3 column. Additionally, the final solutions are carefully degassed in the electrochemical cell with argon for approximately 30 min. The entire electrochemical cell is situated in a glovebag, which is flushed with dry nitrogen to decrease product degradation during the transfer of solutions. The oxidized samples are transferred from the electrolysis cell to the X-ray sample holders and precision EPR tubes using nitrogen-flushed pipettors, and immediately frozen in liquid nitrogen.

Mn K-Edge X-ray Absorption Spectroscopy. Mn K-edge absorption spectra are collected at the wiggler beamline 7−3 at Stanford Synchrotron Radiation Laboratory (SSRL) with SPEAR operating at ring currents of 40−100 mA at 3.0 GeV. The X-ray beam is used unfocused, with an energy-scanning Si[220] double-crystal monochromator detuned to 50% to attenuate higher harmonics.[48] The Mn absorption spectra are recorded as fluorescence excitation spectra,[33] using an energy-resolving 13-element Ge detector (Canberra Instruments).[49] Ionization-chamber detectors (I_0, I_1, and I_2) are filled with dinitrogen gas. Absorption is related to the fluorescence signal divided by the incident flux ($A = F/I_0$).[33] A $KMnO_4$ standard, placed between the rear ionization chambers I_1 and I_2, is used to monitor the energy calibration and resolution. The $KMnO_4$ standard has a narrow pre-edge line at 6543.3 eV, the full width at half-height is less than 1.7 eV in the absorption spectrum ($\log(I_1/I_2)$). To reduce radiation damage, samples are kept in a gaseous helium atmosphere at ambient pressure and at a temperature of 10 ± 1 K, using a liquid helium flow cryostat (Oxford Instruments, CF 1208).

XANES spectra are collected from 6520 to 6580 eV, with a step size of 0.2 eV. Reproducibility of the Mn K-edge energy in these conditions is typically ± 0.1 eV.[24] Data analysis for the Mn K-edge XANES has been published earlier[24,48,50] and is described here briefly. A linear pre-edge background is removed from the XANES spectra. Subsequently, the post-edge region (6630−7100 eV) is fit with a quadratic polynomial and normalized to the absorption of one free Mn atom, that is the intensity of the polynomial at 6558 eV is set to 1. For XANES, the first inflection-point energy (IPE) of the second-derivative spectrum is taken as an indicator of the Mn K-edge energy for each compound. Derivatives of the spectra are obtained by analytically deriving a third-order polynomial fit to the data over a sliding ±3.0 eV interval for each data point. There were no differences in the results or the conclusions when a ±1.5 eV interval was used.

Mn Kβ X-ray Emission Spectroscopy. Kβ XES spectra are collected at the wiggler beamline 10−2 at Stanford Synchrotron Radiation Laboratory (SSRL) with SPEAR operating at ring currents of 40−100 mA at 3.0 GeV. The X-ray beam at 9.2 keV is focused to a 1 mm × 4 mm spot, with a flux of approximately 3×10^{11} photons s^{-1}. Samples are positioned at a 45° angle to the X-ray beam. Variations in the incident beam intensity (I_0) are monitored using an ionization-chamber detector filled with dinitrogen gas. The fluorescence emission spectra are measured using a high-resolution crystal-array spectrometer, which consists of a solid-state detector positioned in the focus of eight Bragg-diffracting Si(440) crystals.[51] The resolution under our experimental conditions is ∼1.0 eV; a detailed description is given in Bergmann et al.[51] Samples are protected from radiation damage by keeping them in a gaseous helium atmosphere at ambient pressure and at a temperature of 10 ± 1 K, using a liquid helium flow cryostat (Oxford Instruments CF 1208). Energy calibration and reproducibility are monitored by assigning the first momement of a solid Mn_2O_3 sample to 6490.403 eV. Using these procedures an energy-determination accuracy of ≤0.01 eV within a run and ≤0.03 eV between runs is achieved. The di-μ-oxo compound spectra were collected in a separate run from the mono-μ-oxo compound spectra.

Kβ XES spectra are collected from 6467.2 to 6510.9 eV at 5 s/point. The step size ranges from 0.1 to 0.24 eV. The Kβ XES spectra of the dilute compounds have a linear background resulting from Compton

(46) Schnepf, R.; Sokolowski, A.; Müller, J.; Bachler, V.; Wieghardt, K.; Hildebrandt, P. *J. Am. Chem. Soc.* **1998**, *120*, 2352−2364.

(47) Cooper, S. R.; Dismukes, G. C.; Klein, M. P.; Calvin, M. *J. Am. Chem. Soc.* **1978**, *100*, 7248−7252.

(48) DeRose, V. J.; Mukerji, I.; Latimer, M. J.; Yachandra, V. K.; Sauer, K.; Klein, M. P. *J. Am. Chem. Soc.* **1994**, *116*, 5239−5249.

(49) Cramer, S. P.; Tench, O.; Yocum, M.; George, G. N. *Nucl. Instrum. Methods Phys. Res. A* **1988**, *266*, 586−591.

(50) Latimer, M. J.; DeRose, V. J.; Mukerji, I.; Yachandra, V. K.; Sauer, K.; Klein, M. P. *Biochemistry* **1995**, *34*, 10898−10909.

(51) Bergmann, U.; Cramer, S. P. In *SPIE Conference on Crystal and Multilayer Optics*; SPIE: San Diego, CA, 1998; Vol. 3448, pp 198−210.

Table 1. $Mn^{III}Mn^{IV}$ and Mn^{II} Fractions Calculated from EPR Spectra of the Di-μ-oxo and Mono-μ-oxo Sample Solutions at Different Stages in the Electrochemistry (See Also Figures 3 and 4)[a]

	di			mono						
	(III,IV)	(IV,IV)		(III,IV)	(IV,IV)					
		A	B		A	B	C	D	E	F
$Mn^{III}Mn^{IV}$	1	0.19	0.04	0.77	0.85	0.48	0.25	0.15	0.09	0.05
Mn^{II}	–	–	–	–	0.01	0.02	0.02	0.02	0.03	0.03

[a] In the nomenclature of the electrochemical samples, "di" refers to the di-μ-oxo compound, and "mono" refers to the mono-μ-oxo compound. The Roman numerals between brackets indicate the desired oxidation state of the compound. Different extraction time-points are indicated by A through F.

scattering. This background is determined by aligning spectral regions that are oxidation-state independent, that is, outside the 6470−6505 eV range, to those of concentrated Mn oxides (MnO, Mn_2O_3, and MnO_2). The result is then fit with a linear function and subtracted from the experimental data. To simplify mathematical operations, the spectra are splined onto a grid of 0.1 eV energy steps. Concomitantly, the integrated area from 6468 to 6510 eV of each spectrum is normalized to 1. The first moment, $\langle E \rangle$, of the K$\beta_{1,3}$ peak is calculated between 6485 and 6495 eV using eq 1, and is used as an energy indicator.

$$\langle E \rangle = \frac{\sum_i E_i \cdot I_i}{\sum_i I_i} \qquad (1)$$

where I_i is the background-corrected emission intensity at each energy E_i.

Results

Analysis of the Electrochemical Solutions. The EPR spectrum of the **di(III,IV)** sample matches the published spectrum for the $Mn^{III}Mn^{IV}$ di-μ-oxo compound in acetonitrile.[47] Only a small amount of the $Mn^{III}Mn^{IV}$ species signal remains in the **di(IV,IV)$_B$** EPR spectrum (Supporting Information). Table 1 and Figure 3 show that, during the electrolysis, the Mn^{III}-Mn^{IV} fraction decreases over time to 0.19 and 0.04 for the **di-(IV,IV)$_A$** and **di(IV,IV)$_B$** samples, respectively.

The degree of conversion during the first oxidation step of the mono-μ-oxo compound is calculated from an UV/vis spectrum of sample **mono(III,IV)** (Supporting Information) and published absorption coefficient data of the $Mn^{III}Mn^{III}$ and $Mn^{III}Mn^{IV}$ species.[2] A least-squares fit is used for the UV/vis absorption values at 335, 380, 400, 480, 495, and 550 nm, and the $Mn^{III}Mn^{III}$:$Mn^{III}Mn^{IV}$ ratio is calculated to be 23:77 (±7). This shows that the first oxidation step is not complete for sample **mono(III,IV)**, as indicated in Figure 4.

The decrease in $Mn^{III}Mn^{IV}$ during the second oxidation step of the mono-μ-oxo compound is followed by EPR spectroscopy, analogous to the di-μ-oxo compound. The $Mn^{III}Mn^{IV}$ EPR signal in the **mono(IV,IV)$_F$** sample spectrum is greatly decreased (Supporting Information). However, the EPR spectrum of the **mono(IV,IV)$_F$** contains an additional six-line EPR signal, which resembles that of free Mn^{II} in acetonitrile. This shows that a small amount of the newly formed $Mn^{IV}Mn^{IV}$ species has decomposed into Mn^{II}. The fractions of the $Mn^{III}Mn^{IV}$ species and Mn^{II} present in the **mono(IV,IV)** samples are determined by least-squares fitting the EPR spectra. Table 1 presents the contribution of the **mono(III,IV)** and Mn^{II} spectra to the various **mono(IV,IV)** sample spectra. The $Mn^{III}Mn^{IV}$ fraction increases first during the second oxidation step (sample **mono(IV,IV)$_A$**) before it decreases (samples **mono(IV,IV)$_B$** to **mono(IV,IV)$_F$**).

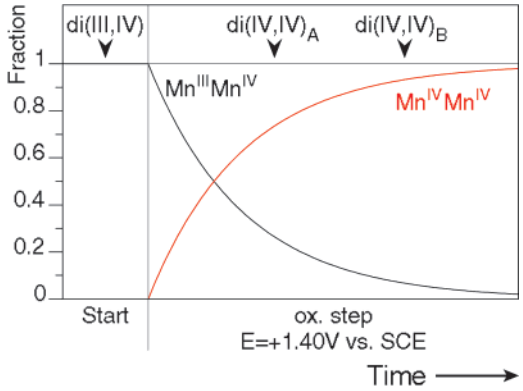

Figure 3. Scheme of the time course for the oxidation reaction of the di-μ-oxo compound. The arrows indicate sample extractions. The $Mn^{III}Mn^{IV}$ compound (**di(III,IV)**) is an EPR-active di-μ-oxo species. The $Mn^{IV}Mn^{IV}$ species is stable and EPR-silent. The EPR spectra of the **di(IV,IV)** samples are analyzed to determine the decline in the $Mn^{III}Mn^{IV}$ concentration. The EPR spectrum of the starting sample (**di(III,IV)**) is used as the pure $Mn^{III}Mn^{IV}$ quantitative standard. In the nomenclature of the electrochemical samples, "**di**" refers to the di-μ-oxo compound. The Roman numerals between brackets indicate the desired oxidation state of the compound. Different extraction time-points are indicated by subscripts.

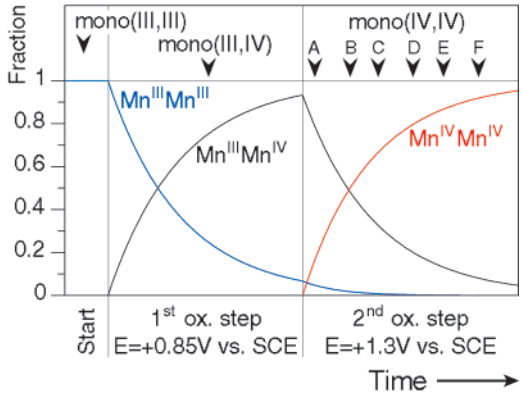

Figure 4. Scheme of the time course for the oxidation reaction of the mono-μ-oxo compound. The arrows indicate sample extractions. UV/vis absorption coefficients of the $Mn^{III}Mn^{III}$ and $Mn^{III}Mn^{IV}$ compounds are used to determine the starting concentration (**mono(III,III)**), and the degree of completion of the first oxidation step (**mono(III,IV)**). The $Mn^{III}Mn^{IV}$ compound is the only EPR-active mono-μ-oxo species; it has a distinctive 18-line spectrum. When water is present in the electrochemical solution, the $Mn^{IV}Mn^{IV}$ species decomposes into Mn^{II}, which has a distinctive six-line EPR spectrum. Therefore, the EPR spectra of the **mono(IV,IV)** samples are analyzed to determine the decline in the $Mn^{III}Mn^{IV}$ concentration and the appearance of the decomposition product Mn^{II}. The EPR spectrum of sample **mono(III,IV)** is used as the $Mn^{III}Mn^{IV}$ quantitative standard, and a $MnCl_2$ acetonitrile solution as the Mn^{II} quantitative EPR standard. In the nomenclature of the electrochemical samples, "**mono**" refers to the mono-μ-oxo compound. The Roman numerals between brackets indicate the desired oxidation state of the compound. Different extraction time-points are indicated by subscripts.

This initial increase is due to the incomplete first oxidation step, as was determined by UV/vis spectroscopy (see also Figure 4). Table 1 also shows that only a very small fraction (3%) of $Mn^{IV}Mn^{IV}$ species decomposes into Mn^{II}. Table 2 gives the oxidation state fractions of the di-μ-oxo and mono-μ-oxo samples used to deconvolute the measured sample X-ray spectra into pure oxidation-state spectra.

From the X-ray crystallographic data, it is known that no major structural changes in the compounds occur upon oxida-

Table 2. Fractions of the Manganese Components Used to Deconvolute the Measured EXAFS, XANES, and Kβ XES Spectra into Pure Oxidation-State Spectra of the Mono-μ-oxo and Di-μ-oxo Compounds

		$Mn^{III}Mn^{III}$	$Mn^{III}Mn^{IV}$	$Mn^{IV}Mn^{IV}$	Mn^{II}
di	(III,IV)	–	1.0	–	–
	$(IV,IV)_B$	–	0.04 ± 0.01	0.96 ± 0.01	–
mono	(III,III)	1.0	–	–	–
	(III,IV)	0.23 ± 0.07	0.77 ± 0.07	–	–
	$(IV,IV)_F$	–	0.05 ± 0.01	0.92 ± 0.02	0.03 ± 0.01

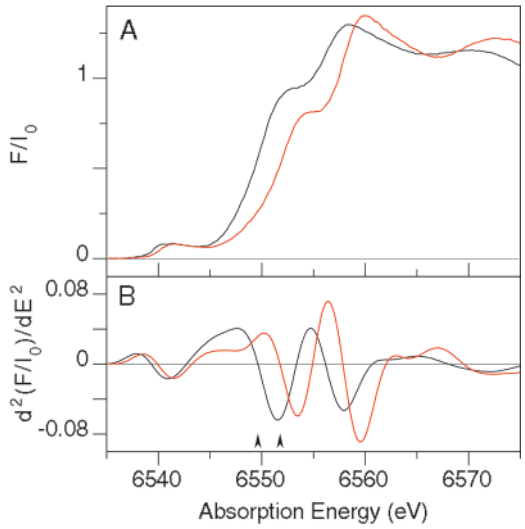

Figure 5. The deconvoluted Mn K-edge XANES (A) and second-derivative (B) spectra of the di-μ-oxo compound in its two oxidation states: $Mn^{III}Mn^{IV}$ (black) and $Mn^{IV}Mn^{IV}$ (red). The arrows in the second-derivative spectra indicate the first-inflection point energy for the two oxidation states: $Mn^{III}Mn^{IV}$ = 6549.6 eV and $Mn^{IV}Mn^{IV}$ = 6551.8 eV.

tion.[1,2] The EXAFS spectra of the samples confirm these expectations. The Mn−Mn backscatter Fourier peak is present in all of the spectra, indicating that the μ-oxo bridges remain intact. Changes are observed in the Mn−N/O Fourier peak, which can be explained by changes in bond distances due to the redox reactions (Supporting Information).

Analysis of XANES and Kβ XES data. The Mn K-edge XANES and the second-derivative spectra of the di-μ-oxo and mono-μ-oxo compounds are shown in Figures 5 and 6. Oxidation of Mn^{III} to Mn^{IV} for each compound causes all K-edges to shift to a higher energy and change in shape slightly. This behavior is reversible; that is, when the higher oxidation states are reduced, the Mn K-edges shift to lower energy (data not shown). The magnitude of the shift depends on the type of compound. A measure of the magnitude of edge shifts are the changes in first inflection point energies (IPEs), which are indicated by the arrows in Figures 5B and 6B and summarized in Table 3. The Mn K-edge shift for the oxidation of the di-μ-oxo compound ($Mn^{III}Mn^{IV} \rightarrow Mn^{IV}Mn^{IV}$) is 2.2 eV. The shift in energy for the first oxidation step of the mono-μ-oxo compound ($Mn^{III}Mn^{III} \rightarrow Mn^{III}Mn^{IV}$) is 1.2 eV, and it is 0.7 eV for the second oxidation step ($Mn^{III}Mn^{IV} \rightarrow Mn^{IV}Mn^{IV}$). Each shift is smaller than that observed for the di-μ-oxo compound. The pre-edge features also change upon oxidation of the compounds. The shift in the pre-edge IPE for the di-μ-oxo compound is 0.6 eV. For the first oxidation step of the mono-μ-oxo compound this shift is 0.7 eV, similar to that of the di-μ-oxo compound. However, the shift in pre-edge IPE for the second oxidation step is only 0.1 eV. The shape of the Mn K-edge is also highly

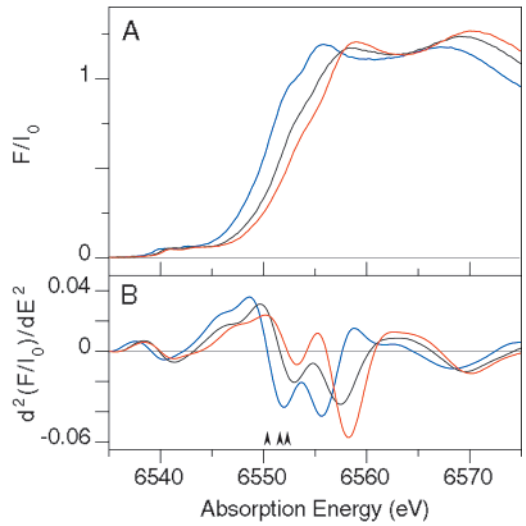

Figure 6. The deconvoluted Mn K-edge XANES (A) and second-derivative (B) spectra of the mono-μ-oxo compound in its three oxidation states: $Mn^{III}Mn^{III}$ (blue), $Mn^{III}Mn^{IV}$ (black), and $Mn^{IV}Mn^{IV}$ (red). The arrows in the second-derivative spectra indicate the first inflection-point energy for each of the three oxidation states: $Mn^{III}Mn^{III}$ = 6550.4 eV, $Mn^{III}Mn^{IV}$ = 6551.6 eV, and $Mn^{IV}Mn^{IV}$ = 6552.3 eV.

dependent on the type of compound. In comparison to the di-μ-oxo species, the mono-μ-oxo species Mn K-edges have less structure.

The difference Mn K-edge XANES spectra for the oxidation-state transitions are presented in Figure 7. The difference spectra show similar structures for the oxidation-state transitions of each compound, that is, two broad negative peaks in the 6545−6558 eV range and a weak broad positive peak at 6561 eV. However, the energy and intensity of the peaks depend on the ligand environment and starting oxidation state of the compound. The di-μ-oxo compound also shows a feature at ~6540.0 eV in the pre-edge region. The first oxidation step of the mono-μ-oxo compound shows a feature at ~6539.8 eV, with a smaller intensity than that of the di-μ-oxo compound. No significant change is observed in the pre-edge region for the second oxidation step of the mono-μ-oxo compound.

Figure 8 presents the Kβ XES spectra of the di-μ-oxo (A) and mono-μ-oxo (B) compounds in their respective oxidation states. The weaker Kβ' peak is at ~6476 eV, and the stronger K$\beta_{1,3}$ peak occurs at ~6491 eV.[39] The insets present the K$\beta_{1,3}$ emission on an expanded scale. Figure 8 shows that, upon oxidation of the di-μ-oxo and mono-μ-oxo compounds, the K$\beta_{1,3}$ peak shifts to a lower energy. First moments are used to quantify the magnitude of the shift of the K$\beta_{1,3}$ peak; they are summarized in Table 3. The shift in first moments is ~0.21 eV to lower energy for each oxidation step, indicating that the changes observed between the compounds are very similar. Support for this observation is shown in Figure 9, which presents the Mn K$\beta_{1,3}$ XES difference spectra of the oxidation steps of the compounds. The K$\beta_{1,3}$ XES difference spectra are all similar in shape, intensity, and energy, within the error of the measurements. Each difference spectrum shows an increase in intensity at ~6490 eV and a decrease at ~6492 eV upon oxidation, with a zero-crossing of ~6491 eV.

Discussion

Deconvolution into Pure Oxidation-State Spectra. The trends observed in the XANES and Kβ XES spectra rely on the quality of deconvolution of the measured data into pure

Table 3. Summary of the First Inflection-Point Energy (1st IPE) Values of the Pre-Edge, and Main Mn K-Edge of the Second-Derivative XANES Spectra of the Mono-μ-oxo and Di-μ-oxo Compounds in Their Pure Oxidation States, as Well as a Synopsis of the First Moments of the K$\beta_{1,3}$ Peaks of the Mono-μ-oxo and Di-μ-oxo Compound in Their Pure Oxidation States[a]

		Mn K-edge XANES				Mn Kβ XES	
compound		pre-edge IPE (eV)	Δ (eV)	edge 1st IPE (eV)	Δ (eV)	1st moment K$\beta_{1,3}$ (eV)	Δ (eV)
di-μ-oxo	III,IV	6539.3 $\pm$ 0.1	0.6	6549.6 $\pm$ 0.1	2.2	6490.21 $\pm$ 0.01	−0.20
	IV,IV	6539.9 $\pm$ 0.1		6551.8 $\pm$ 0.1		6490.01 $\pm$ 0.01	
mono-μ-oxo	III,III	6539.1 $\pm$ 0.1	0.8	6550.4 $\pm$ 0.1	1.2	6490.39 $\pm$ 0.01	−0.21
	III,IV	6539.9 $\pm$ 0.1		6551.6 $\pm$ 0.2		6490.18 $\pm$ 0.03	
	IV,IV	6540.0 $\pm$ 0.1	0.1	6552.3 $\pm$ 0.2	0.7	6489.96 $\pm$ 0.03	−0.22

[a] The di-μ-oxo compound and mono-μ-oxo compound spectra were collected during different runs. Therefore, when the K$\beta_{1,3}$ first moments of the mono-μ-oxo compound are compared to those of the di-μ-oxo compound, an error of $\pm$0.02 eV is present in addition to the error values shown.

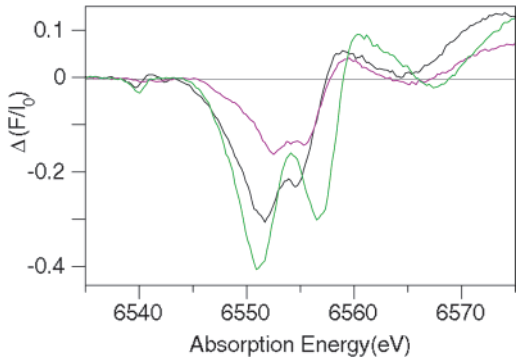

Figure 7. The deconvoluted Mn K-edge difference spectra for the different oxidation state transitions of the di-μ-oxo compound; $Mn^{IV}Mn^{IV} - Mn^{III}Mn^{IV}$ (green), and of the mono-μ-oxo compound: $Mn^{III}Mn^{IV} - Mn^{III}Mn^{III}$ (black) and $Mn^{IV}Mn^{IV} - Mn^{III}Mn^{IV}$ (purple).

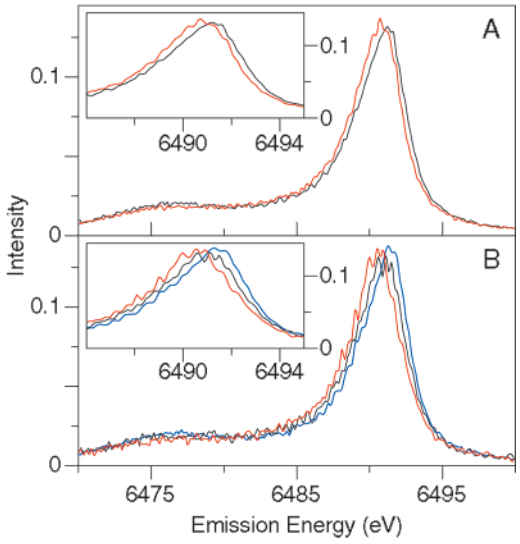

Figure 8. The deconvoluted Kβ XES of the di-μ-oxo compound (A) and the mono-μ-oxo compound (B) in their respective oxidation states: $Mn^{III}Mn^{III}$ (blue), $Mn^{III}Mn^{IV}$ (black), and $Mn^{IV}Mn^{IV}$ (red). The spectra show the entire spectral region with the two emission bands: Kβ' (weak, left) and K$\beta_{1,3}$ (strong, right). The insets show the Mn K$\beta_{1,3}$ XES spectra on an expanded scale.

oxidation compound spectra. The accuracy of the deconvolution is highly dependent on the degree of completion of the electrochemical reactions. A completion of about 96% is achieved for the oxidation of the di-μ-oxo compound (Table 2). Therefore, the correction needed to obtain the deconvoluted pure oxidation-state X-ray spectra is minor. The change in IPE (XANES) and 1st-moment (Kβ XES) values are less than the inherent errors of each method when the raw and deconvoluted data are compared (see Supporting Information).

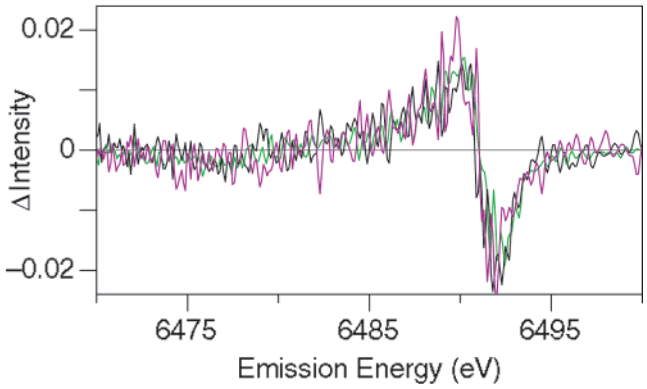

Figure 9. The deconvoluted Kβ XES difference spectra for the different oxidation-state transitions of the di-μ-oxo compound: $Mn^{IV}Mn^{IV} - Mn^{III}Mn^{IV}$ (green), and of the mono-μ-oxo compound: $Mn^{III}Mn^{IV} - Mn^{III}Mn^{III}$ (black) and $Mn^{IV}Mn^{IV} - Mn^{III}Mn^{IV}$ (purple).

The first oxidation step of the mono-μ-oxo compound is the least complete of all of the oxidation reactions (77%). Nevertheless, the correction needed to obtain the pure $Mn^{III}Mn^{IV}$ oxidation state X-ray spectra is small. Differences of 0.3 eV in IPE (XANES) and 0.05 eV in first-moment (Kβ XES) values are observed when the raw and deconvoluted spectra are compared (Supporting Information). The conversion during the second oxidation step is almost complete for the **mono(IV,IV)$_F$** sample (92% $Mn^{IV}Mn^{IV}$). Therefore, only minor corrections for the incomplete oxidation and decomposition are needed to obtain the pure $Mn^{IV}Mn^{IV}$ oxidation-state X-ray spectra (the correction fractions of the $Mn^{IV}Mn^{IV}$ species and Mn^{II} are in Table 2). When the raw and deconvoluted spectra are compared (see Supporting Information), a change of 0.3 eV in the IPE (XANES) value is observed, and only a 0.05 eV change in first-moment (Kβ XES) value. The Fourier transformed EXAFS spectra confirmed that the Mn−Mn backscatter peak at R′ > 2.0 Å remains intact, and the di-μ-oxo and mono-μ-oxo samples consist of manganese dimers. No major structural changes occur upon oxidation of the two compounds.

Oxidation-State Changes and Ligand Effects on XANES and Kβ XES Spectra. The Mn K-edge XANES spectra shift to higher energy upon each oxidation step of the mono-μ-oxo ($[Mn^{III}]_2 \rightarrow Mn^{III}Mn^{IV} \rightarrow [Mn^{IV}]_2$) and di-$\mu$-oxo compound ($Mn^{III}Mn^{IV} \rightarrow [Mn^{IV}]_2$). This is expected, because the overall charge of the atom increases when a manganese atom is oxidized. Consequently, more energy is required to excite an electron from the 1s to the 4p or higher orbitals.[29,52,53]

(52) Cramer, S. P. In *X-ray Absorption: Principles, Applications, Techniques of EXAFS, SEXAFS and XANES*; Koningsberger, D. C., Prins, R., Eds.; Wiley: New York, 1988; p 257.

(53) Yachandra, V. K. In *Methods in Enzymology*; Sauer, K., Ed.; Academic Press: 1995; Vol. 246, pp 638−675.

The Mn K-edge energy and shape do not depend solely on the oxidation state of the manganese atoms (Figures 5 and 6), but also on the ligand environment. This is caused by mixing of the ligand and the manganese atomic orbitals.[52] It is possible that a change in structure and ligand environment will have an even greater influence on the main-edge energy and shape than a change in oxidation state. For example, it would be expected from an oxidation state point-of-view that the $Mn^{III}Mn^{IV}$ di-μ-oxo compound edge would have a higher energy than that of the $Mn^{III}Mn^{III}$ mono-μ-oxo compound. However, as shown in Table 3, the $Mn^{III}Mn^{III}$ mono-μ-oxo compound has a higher IPE value than the $Mn^{III}Mn^{IV}$ di-μ-oxo species. This difference in edge energy (and shape) is caused by differences in structure and ligand environment between the di-μ-oxo and mono-μ-oxo compounds. For example, in case of the linear mono-μ-oxo species, the bridging oxygen has the unusual hybridization of *sp*, which is different from the bridging oxygens in the di-μ-oxo compound or even other mono-μ-oxo compounds.[14] Therefore, the mixing of the oxygen and the manganese orbitals is different, and consequently the region and shape of the K-edge will differ. In addition to these major differences in the bridging oxygen ligands, there are also differences in the terminal ligands of the di-μ-oxo and mono-μ-oxo compound. The di-μ-oxo compound has only aromatic terminal ligands, while the mono-μ-oxo compound has a mixture of aromatic and nonaromatic ligands. Aromatic ligands have unoccupied π* orbitals which can have strong π back-bonding interactions with the manganese d orbitals. These interactions are different for nonaromatic orbitals. Therefore, the shape and region of the XANES spectra are also dependent on the terminal ligands.

All oxidation steps of the mono-μ-oxo and di-μ-oxo compounds involve removal of an electron from Mn^{III} to produce Mn^{IV}, without any major changes in ligand environment (see also Analysis of EXAFS in the Supporting Information).[40−43] Therefore, no major changes are expected for the difference spectra of the two oxidation steps of mono-μ-oxo compound. However, Figure 7 shows that the shape, intensity, and peak energy of the main XANES K-edge difference features do depend on the starting oxidation state of the compound. The same applies to the pre-edge, where, in the case of the mono-μ-oxo compound, a difference feature is observed for the first oxidation step ($[Mn^{III}]_2 \rightarrow Mn^{III}Mn^{IV}$). However, no such feature is observed for the second oxidation step ($Mn^{III}Mn^{IV} \rightarrow [Mn^{IV}]_2$). This dependence of the difference spectra on the kind of oxidation step indicates that the two Mn atoms are affecting each other in some way. This behavior can be explained in two possible ways: differences in delocalization of charge or exchange coupling through the bridging oxygen(s). If valence delocalization occurs, the first oxidation step should present a $[Mn^{3+}]_2 \rightarrow [Mn^{3.5+}]_2$ transition, and the second oxidation step would present a $[Mn^{3.5+}]_2 \rightarrow [Mn^{4+}]_2$ transition. This could explain the changes in difference spectra between the two oxidation steps, because the two oxidation steps are not the same. However, Horner et al.[2] found that the mono-μ-oxo oxidation-state species are valence-trapped (Robin-Day class I[54]). Therefore, the interaction between the Mn atoms needs to happen via the bridging oxygen. This explanation is supported by the fact that the mono-μ-oxo species are strongly antiferromagnetically coupled.[2] This again exemplifies how important the bridging ligands can be to the changes observed in the Mn K-edge XANES spectra upon oxidation.

The first moments of the K$\beta_{1,3}$ peak energy are equal, within the error of the method, for the mono-μ-oxo and the di-μ-oxo compound in their $Mn^{III}Mn^{IV}$ or $Mn^{IV}Mn^{IV}$ oxidation state (Table 3, add $\pm$0.02 eV to error values when di-μ-oxo and mono-μ-oxo are compared). This indicates that the energy of the K$\beta_{1,3}$ peak is determined mostly by the oxidation state of the manganese atom rather than the ligand environment. This is also evident from the difference spectra of the mono-μ-oxo and the di-μ-oxo compound (Figure 9). Not only are the energies of the maximum, minimum, and zero crossing the same for the difference spectra of all of the oxidation transitions, but the intensity is also similar. This also shows that the change in shape of the K$\beta_{1,3}$ peak is less ligand-dependent than it is for XANES. Kβ XES reflects the transition of a 3p electron to a 1s hole.[28] The energy of the 3p level is affected by the magnitude of the 3p−3d exchange interaction. This exchange interaction is mainly determined by the number of unpaired electrons in the 3d level and is less affected by changes in the energy of the 3d levels due to ligand-field interactions. In addition, the 3p orbitals are smaller than the 3d and 4p orbitals, and therefore have less overlap with the 2p and π orbitals of the ligand environment. Thus, the 3p orbitals (Kβ XES) are less sensitive to the ligand environment than the 4p orbitals (XANES).

Conclusions

Due to the purity, low degree of decomposition, and high degree of completion of the oxidation reactions the measured data needed only small corrections to obtain the pure oxidation-state spectra for each compound. This is evident from the minor differences between measured and deconvoluted data. This enabled us to study the dependence of Mn K-edge XANES and Mn Kβ XES spectra on ligand environment and oxidation state for these two specific compounds in solution with a high degree of reliability.

The Mn K-edge XANES spectra give information on both the oxidation state of the manganese atoms and on their ligand environment. These spectra show energy shifts of 0.7−2.2 eV for oxidation-state changes and 0.5−2.0 eV for ligand-environment changes. This dependence on oxidation state and ligand environment is especially evident in the XANES difference spectra. Therefore, care must be exercised when correlating the Mn K-edge energies to manganese oxidation states without taking into account the nature of the ligand environment. This is especially a problem when sets of compounds with different ligand structures, different nuclearities, and different analysis methods to determine edge positions are used to infer oxidation-state information about biological systems, such as in Kuzek et al.[55] However, there is a correlation between manganese oxidation state and Mn K-edge energy if the ligand environment stays the same; the edge shifts to a higher energy upon oxidation within a given compound. No such correlation exists for the pre-edge feature, which shows an energy shift of 0.8 eV for the first oxidation step of the mono-μ-oxo compound, but only 0.1 eV for the second oxidation step. This difference in behavior of the main Mn K-edge and pre-edge is because each feature is due to transitions to different molecular orbitals.

The Kβ XES spectra show an energy shift of ~0.21 eV for oxidation state-changes and only ~0.04 eV for ligand-environment changes. Therefore, this method is less dependent on the ligand environment of the manganese atoms than on the oxidation states. Additional compounds are being studied to see whether there is indeed such a strong correlation between oxidation state and K$\beta_{1,3}$ peak energy. Furthermore, multiplet calculations are being performed to enhance our theoretical

(54) Robin, M. B.; Day, P. *Adv. Inorg. Chem. Radiochem.* **1967**, *10*, 247−422.

(55) Kuzek, D.; Pace, R. J. *Biochim. Biophys. Acta* **2001**, *1503*, 123−137.

understanding of Kβ XES spectra. On the basis of currently available data, Kβ XES seems to be an accurate method to determine the oxidation state of manganese atoms, in model compounds and biological systems, such as PS II.[22] The study of the different behavior of the XANES pre-edge and main edge in conjunction with Kβ XES can provide much information about the character of the ligand environment of manganese atoms. In conclusion, Mn K-edge XANES and Kβ XES are complementary methods, which give a wealth of information about oxidation state and ligand environment of the manganese atoms in model compounds and biological systems.[22]

Abbreviations: PS II, Photosystem II; OEC, oxygen-evolving complex; XAS, X-ray absorption spectroscopy; XANES, X-ray absorption near-edge structure; IPE, inflection-point energy; EXAFS, extended X-ray absorption fine structure; XES, X-ray emission spectroscopy; EPR, electron paramagnetic resonance; IR, infrared; SCE, saturated calomel electrode; L′, 1,10-phenanthroline; di-μ-oxo compound, $[L'_2Mn^{III}O_2Mn^{IV}L'_2](ClO_4)_3$; L, *N*,*N*-bis(2-pyridylmethyl)-*N*′-salicylidene-1,2-diaminoethane; mono-μ-oxo compound, $[LMn^{III}OMn^{III}L](ClO_4)_2$; TBA, tertbutylammonium.

Acknowledgment. This paper is dedicated to the memory of Mel Klein, who was the consummate role model as a mentor, scientist, colleague, and friend. We thank Drs. Olivier Horner and Sandrine Poussereau for providing the manganese model compounds. We are grateful to Drs. Johannes Messinger, Roehl M. Cinco, Karen L. McFarlane, Shelly A. Pizarro, and Carmen Fernandez for their long hours on beamlines 7-3 and 10-2 at SSRL. Synchrotron radiation facilities were provided by the Stanford Synchrotron Radiation Laboratory (SSRL) which is operated by the Department of Energy, Office of Basic Energy Sciences. The SSRL Biotechnology Program is supported by the National Institutes of Health, National Center of Research Resources, Biomedical Technology Program, and by the Department of Energy, Office of Biological and Environmental Research. During her stay in Berkeley, E.A.-M. was partly supported by the France-Berkeley Fund. This research was supported by the National Institutes of Health (GM-55302 to V.K.Y., GM-44891-5 and GM-48145 to S.P.C.), and the Director, Office of Basic Energy Sciences, Division of Energy Biosciences of the U.S. Department of Energy (DOE), under Contract DE-AC03-76SF00098.

Supporting Information Available: Experimental details and figures (PDF). This material is available free of charge via the Internet at http://pubs.acs.org.

JA004306H